

Evaluation of printability of crystal growth defects in a 193nm lithography environment using AIMS™

Rainer Schmid^{*a}; Axel M. Zibold^a; Kaustuve Bhattacharyya^b; Xuemei Chen^b; Brian Grenon^c
^aCarl Zeiss SMS GmbH; ^bKLA-Tencor, San Jose; ^cGrenon Consulting, Inc

ABSTRACT

The frequent occurrence of crystal growth defects on the patterned surface and back glass of critical layer reticles in 193nm lithography has been seen at most advanced fabs around the world. While frequent contamination inspections using regimented sample plans help monitor the growth of crystals and protect yield, no clear solutions have been found to eliminate this progressive defect growth.

The recently proposed “Advanced Reticle Defect Disposition Process” (ARDD), was applied successfully for the first time. This process employs a high-throughput inspection system based on the STARlight architecture and - after defect reduction through algorithms - a high-resolution AIMS™ review system, utilizing the newest networked data connectivity to directly exchange inspection report data and review results.

The printability of crystal growth defects is highly variable depending on which surface the defects occur, the size of the defects, and the proximity of the defect to a printing pattern. Crystal growth defects can have different transmittance and phase depending on the lithography wavelength and we found in our investigations a significant change in transmission loss depending on lithography settings like NA and sigma. Such effects may result in severe reduction of the process window, and affect yield.

Progressive reticle defects have been characterized on a production reticle applying the ARDD process. It is shown that emulating any given stepper/ scanner settings is necessary to measure the effect of these types of defects on transmittance and that through-focus AIMS™ evaluation is required to accurately assess the printability of crystal growth defects in terms of process window on wafer. Both features are important components of an overall effective and economical reticle monitor strategy, e.g. in order to optimize the reticle cleaning cycles and thus the reticle lifetime.

Keywords: printability, reticle defects, mask inspection, actinic analysis, 193nm, AIMS™, crystal growth.

1. BACKGROUND

The concept of pellicles (see figure 1) was developed to protect the critical reticle surface against defects like particles and scratches caused by handling [1, 2]. They have been employed successfully for many years to ensure the utilization of the often very expensive reticles in production to the full extend of their lifetime.

With the introduction of DUV lithography processes and specifically the 193nm process, crystal growth defects have emerged as new type of defect occurring underneath the pellicle surface. In fact, they have become the most challenging type of progressing reticle defects in the 193nm production environment over the last years. Although the underlying mechanisms of their generation are meanwhile understood in principle, there are no solutions established to prevent these defects from occurring. Furthermore, some of the components of the adhesives used to keep the pellicle in place as well as the more or less enclosed environment underneath the pellicle seem to enhance the conditions under which these crystal defects form [3]. Due to the significance of this problem at 193-nm scanner wavelength exposure, the authors decided to run some experiments with a focus on establishing the evaluation of aerial image measurements as a method to assess the impact of these types of defects on the process window for wafer prints. The experiment and the results are explained below.

*rainer.schmid@smt.zeiss.com, phone +1 914 906 8534

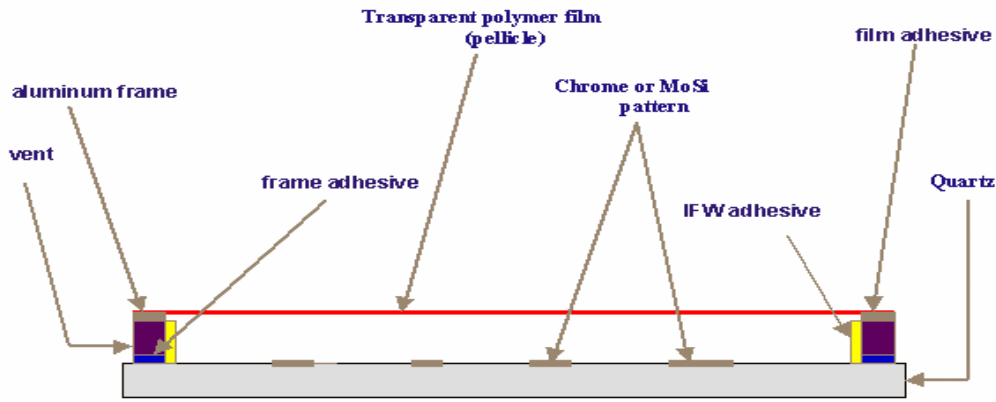


Figure 1: Components of a photo mask with pellicle.

2. THE ADVANCED RETICLE DEFECT DISPOSITION (ARDD) PROCESS

2.1 Advanced Reticle Defect Disposition

Recently the “Advanced Reticle Defect Disposition” (ARDD) process was introduced as a solution to monitor and disposition progressing reticle defects in the wafer fab environment [4]. In this process (see figure 2) the reticle is first inspected with a high throughput inspection system like TeraSTAR applying the STARlight architecture in order to detect all defects present on the reticle surface and generate a list of these defects with precise location information in an inspection report. Through culling algorithms this defect list is reduced only to defects whose impact can not be determined conclusively. To come to an ultimate assessment of these defects they are reviewed in an AIMS™ fab system by evaluating through-focus stacks of the aerial image at the actinic wavelength and determining their impact on the process window. To optimize the information flow between the inspection and AIMS™ systems a special ETHERCOMM interconnectivity protocol was developed to ensure a quick and reliable redetection of these defects.

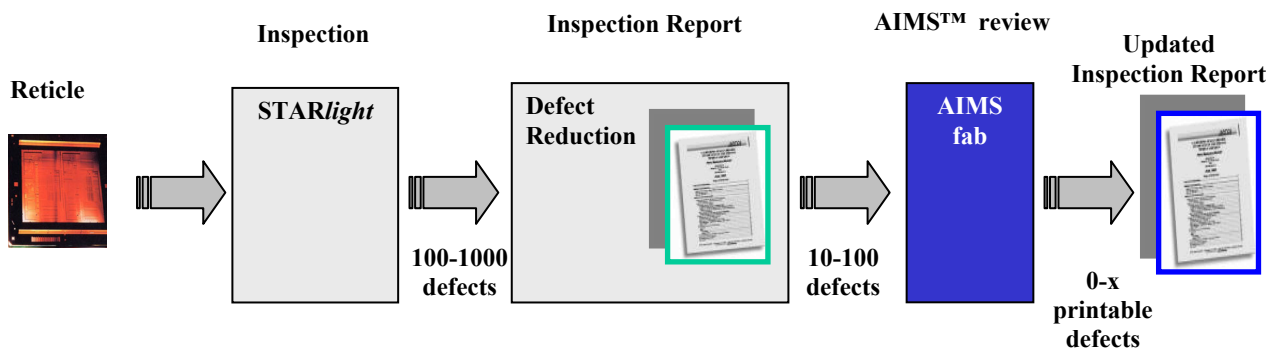


Figure 2: The Advanced Reticle Defect Disposition (ARDD) process.

In this experiment the newly established ETHERCOMM protocol was demonstrated successfully for the first time. This establishes the functionality of exchanging inspection reports through a direct link between the TeraSTAR inspection system and the AIMS™ system including alignment information as well as writing AIMS™ assessment results back to the inspection report. The investigation of the exact parameters of this new process will be the subject of a separate line of experiments.

2.2 Inspection Method

Detection of any defects not only on the clear area of the mask, but also on the attenuator and chrome surfaces of the mask was an important criterion of this experiment. The TeraSTAR (STARlight) inspection system used in this study utilizes simultaneous transmitted and reflected UV illumination and a special contamination detection algorithm to detect particles, stains, thin-chrome, ESD, flat, semi-transparent defects, and transmission errors, both in the clear and opaque areas. A single UV laser source scans the photomask on a perpendicular axis, and two photo-sensors collect the reflected and transmitted light. The two digitized outputs are processed using advanced algorithms and any unexpected condition in the intensities of the detected signals indicates a defect. Thus it was possible to detect any defect increase not only on the clear area of the mask but also on the attenuator and chrome surface of the mask.

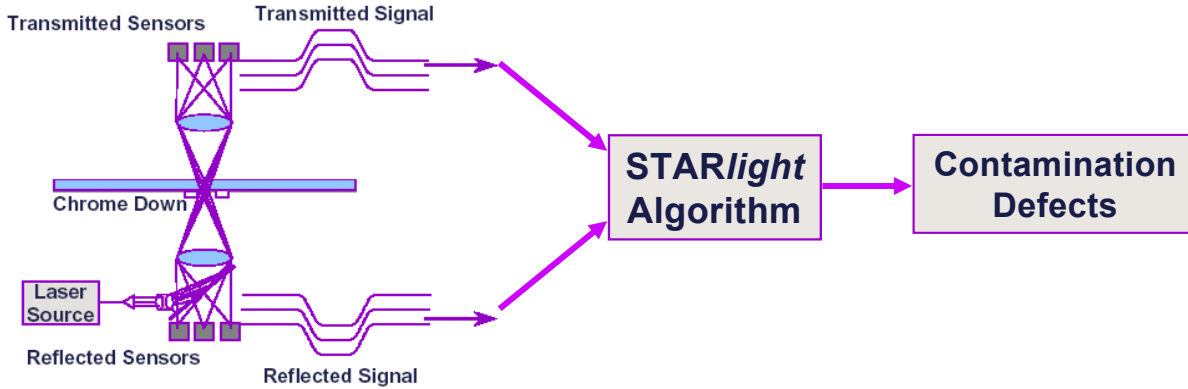


Figure 3: The STARlight architecture.

2.3 AIMS™ Review

AIMS™ is an aerial image measurement system that emulates wafer prints under a wide range of stepper / scanner settings [5, 6]. The aerial image taken with the system is optically equivalent to the latent image incident on the photo resist of the wafer, but magnified and recorded with a CCD camera (see figure 4). The field of view is measured as through-focus stack with several aerial images to provide full depth-of-focus information. The AIMS™ tools are available for different wavelengths (248 nm, 193 nm and 157 nm), the operating wavelength of the AIMS™ 193 plus system used for this experiment is $\lambda = 193\text{nm}$. The lithography parameters on this system can currently be chosen from 0.30 to 0.92 for NA and from 0.30 to 1.0 for sigma. A variety of special illumination types like different annular settings, off-axis, dipole, quadrupole or specific customized illumination settings can be accommodated. The AIMS™ fab 193 system is available with mini-environment and optionally with mask handling from SMIF pods or from specific reticle boxes.

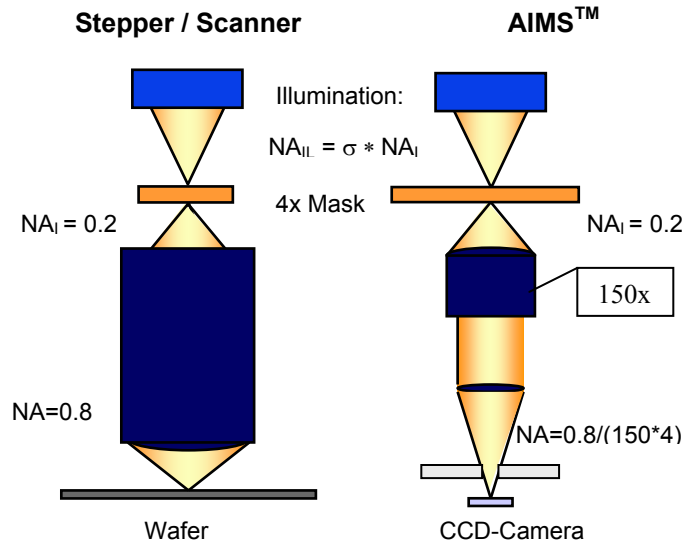


Figure 4: Principle of AIMS™ imaging with example settings.

3. DEFECT COMPOSITION ANALYSIS – RAMAN SPECTROSCOPY

Raman spectroscopy is a light scattering technique complementary to the technique of infrared spectroscopy [7]. Raman spectroscopy provides vibration information about the analyzed compounds. It depends on a change in the induced dipole moment or polarization to produce Raman scattering. When a beam of photons strikes a molecule, the photons are scattered elastically (Rayleigh scattering) and inelastically (Raman scattering) generating Stoke's and anti-Stokes lines (see figure 5).

The Raman spectra were collected using a Renishaw Model 2000 Raman spectrometer equipped with a 633-nm laser. All measurements were made without removing the pellicle. The beam size is approximately 1 μ m in diameter. The results show that there are two major kinds of defects involved – Ammonium Sulfate and Cyanuric Acid (see figures 6 and 7).

Background Raman spectra on the mask surface (at a non-defective spot) were collected from both inside and outside of the pellicle covered area to cancel out the possibility of contamination due to transport and handling.

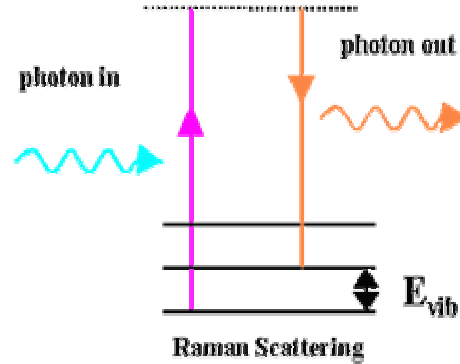


Figure 5: Raman Scattering.

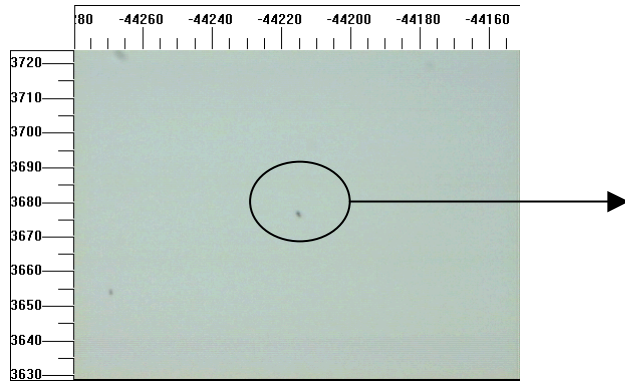


Figure 6: A defect used to collect Raman Spectra.

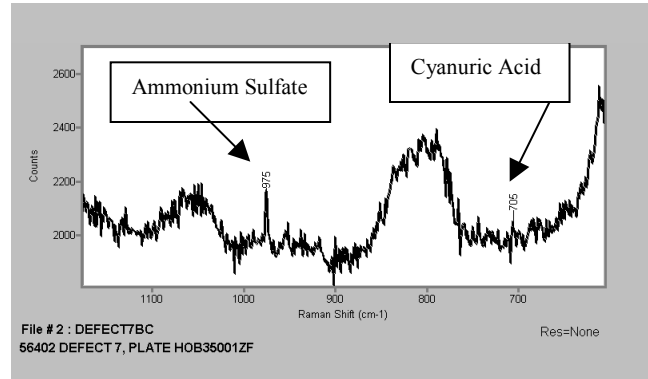


Figure 7: Raman Spectra indicating peaks at 975 cm⁻¹ and 705 cm⁻¹.

4. MEASUREMENT RESULTS AND DISCUSSION

4.1 Inspection Results

Figure 8 shows a screen shot of the STARlight inspection results of one “swath”. A swath is one scanning line of the laser spot across the length of the reticle. Alone in swath # 15 a total count of > 1300 defects was detected. Most of the defects are located in the clear area or at the clear / attenuator interface.

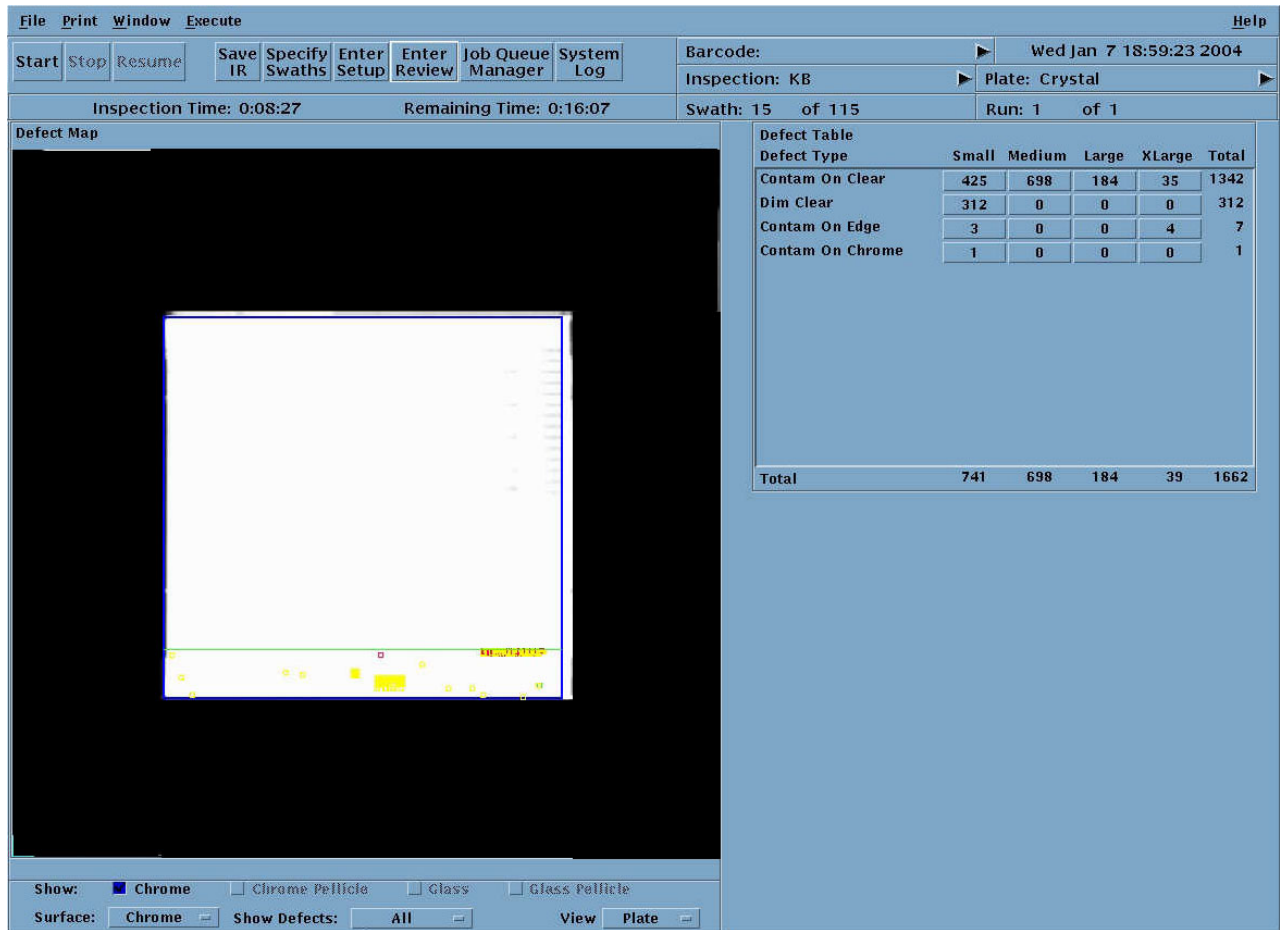


Figure 8: STARlight inspection result showing >1300 crystal defects along one laser scanning line across the reticle.

4.2 AIMS™ measurements

Transmission loss at different lithography settings

For evaluation with the AIMS™ fab 193 plus system, 14 of the detected crystal growth defects on clear were selected randomly out of the vast number of defects on this specific reticle. In this experiment the following lithography settings were selected: “lithography settings 1” emulate stepper/ scanner settings of $NA = 0.75$ and $\sigma = 0.8$ with an annular 2:3 illumination, for “lithography settings 2” the emulated stepper/ scanner settings were $NA = 0.85$ and $\sigma = 0.6$, again with an annular 2:3 illumination.

Table 1 gives an overview of the characterized defects with respect to transmission loss and approximate defect size. Transmission loss as well as defect size are determined through AIMS™ measurements with the two different lithography settings. Transmission loss was calculated as the relative change in normalized intensity and was determined in the best focus plane. The size is the longest extension of each defect in any direction in the AIMS™ image.

Table 1:

Overview of crystal growth defects evaluated with AIMS™ showing transmission loss and approximate size at wafer.
 “Lithography settings 1”: NA = 0.75, sigma = 0.8, annular 2:3 illumination.
 “Lithography settings 2”: NA = 0.85, sigma = 0.6, annular 2:3 illumination.
 The same crystal growth defects show significantly different transmission loss at the different lithography settings.

defect #	lithography settings 1		lithography settings 2	
	size [µm at wafer]	transm. loss [%]	size [µm at wafer]	transm. loss [%]
1	0.50	49	0.48	74
2	0.42	53	0.46	75
3	0.41	70	0.54	89
4	0.65	45	0.68	71
5	0.60	35	0.63	51
6	0.32	60	0.38	80
7	0.36	56	0.37	75
8	0.34	62	0.35	77
9	0.51	45	0.50	69
10	0.47	56	0.50	78
11	1.17	18	1.07	29
12	0.43	51	0.55	73
13	0.39	46	0.39	66
14	0.87	11	0.89	26

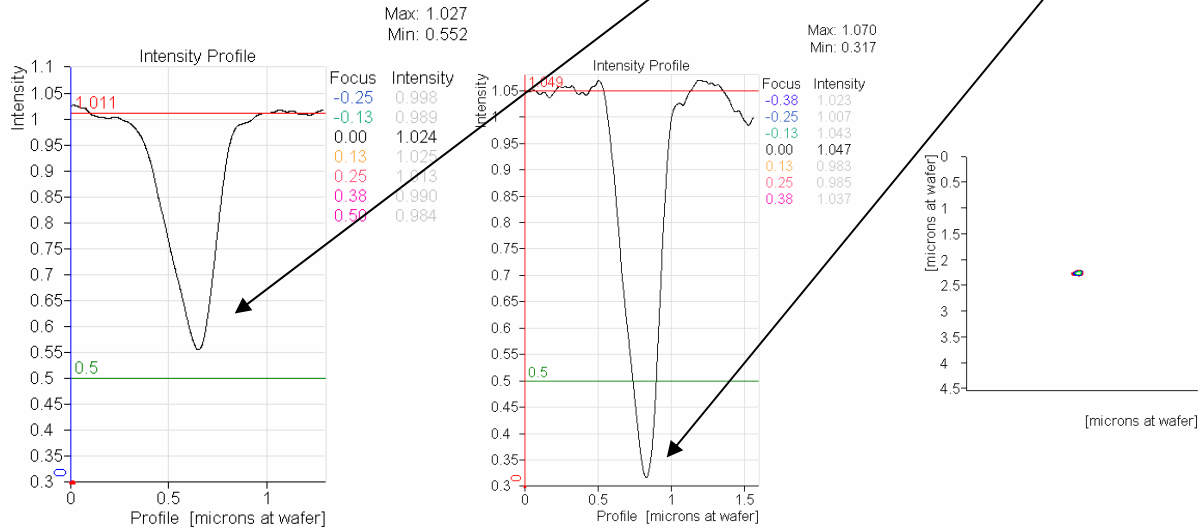


Figure 9: On the left side the intensity plot of defect #9 with lithography settings 1 is displayed. Defining the threshold at 0.5 makes this defect a non-printing defect with these settings. To the right the intensity plot of the same defect with lithography settings 2 is shown. Working with the same threshold makes this defect a printing defect with those settings. With the AIMS™ software package the contour of features for specific settings can be displayed based on a threshold model. To the very right the contour of defect #9 with lithography settings 2 is shown for a threshold of 0.5.

With lithography settings 2 the transmission loss was in general about 20% higher than with lithography settings 1. Altogether two different types of crystal growth defects were observed: 12 of the 14 defect growths were more or less round, sometimes with a comet tail-like extension in one direction and were between 0.3 and 0.6 µm in diameter. Defects #11 and #14 were rod-like in shape with 0.9 and 1.1 µm in length and a width of approximately 0.4 µm. The latter defects showed a significantly lower transmission loss, e.g. 11% and 18% versus a typical transmission loss between 40 and 60% with lithography settings 1 and 26% and 29% versus a typical transmission loss between 60% and 80% with lithography settings 2.

By applying a threshold model to the measurements in the evaluation mode of the AIMS™ software package the printability of defects in terms of threshold and the selected lithography parameters can be assessed. For example defect #9 shows a transmission loss of approximately 45% with lithography settings 1 and a transmission loss of approximately

69% with lithography settings 2. Selecting e.g. a threshold of 0.5 makes this defect a printing defect with lithography settings 1 and a non-printing defect with lithography settings 2 (see figure 9). This emphasizes that generic criteria like defect size are not sufficient to evaluate progressing defects with respect to their impact on printability. Emulation of the real stepper / scanner settings and assessment of their impact on the aerial image is needed to disposition these types of defects in the most effective and overall most economical way.

Process Window evaluation

As shown in the previous section, defects in a clear area have different or no lithographic significance depending on the lithographic settings of the exposure tool. Such type of crystal growth or haze defects can even show more different lithographic impact if they appear in areas where structures are present. There they can influence the printability of features causing not only transmission loss but also phase effects which influence the process latitude of the affected structure or dense area. Utilizing the information obtained by the through-focus stacks, the impact of crystal growth defects on the size of the lithography process window (exposure-defocus-matrix) can be determined. In figure 10a, a significant haze or crystal growth defect can be seen close to a printing structure on the mask and at first look it certainly appears to act as a proximity effect on the structure. In such a case it is very viable to compare the size and position of the process window of this structure with a reference structure from another die or some other point on the mask where no haze effect can be found close by, as can be seen in figure 10c. The comparison of both process windows will allow to clarify the impact of the haze effect on the lithographic printing process.

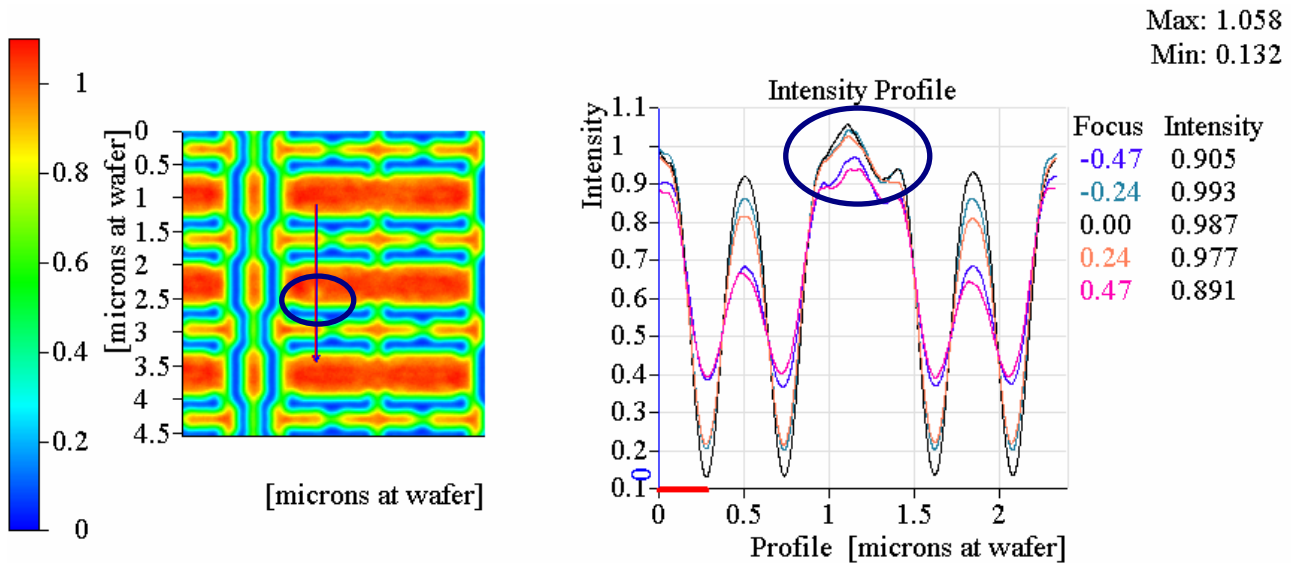


Figure 10a: AIMS™ image and transmission profile of a crystal growth defect close to a printing pattern.

Figure 10b shows the image of the crystal growth defect close to printing patterns (image B) and the same pattern on a different position on the mask without defect (image A). In our example the threshold was selected in the reference feature according to the target CD value in a straightforward threshold model. The process window of reference and structure with haze in the neighborhood overlap well (figure 10c). This means the crystal growth defect in question – which looked considerable - has negligible impact on the lithography printing process and the reticle could still be used as is. From this example it is evident that a judgment based on pure imaging in best focus will not be sufficient. Only the judgment of printability based on through-focus measurements will reveal how large the deviations are in the process windows and what common size can be found. For a quick visualization of the latent resist image the contour plot which is based on a straightforward threshold model can be used to show that this defect is a non-printing defect (figure 10d).

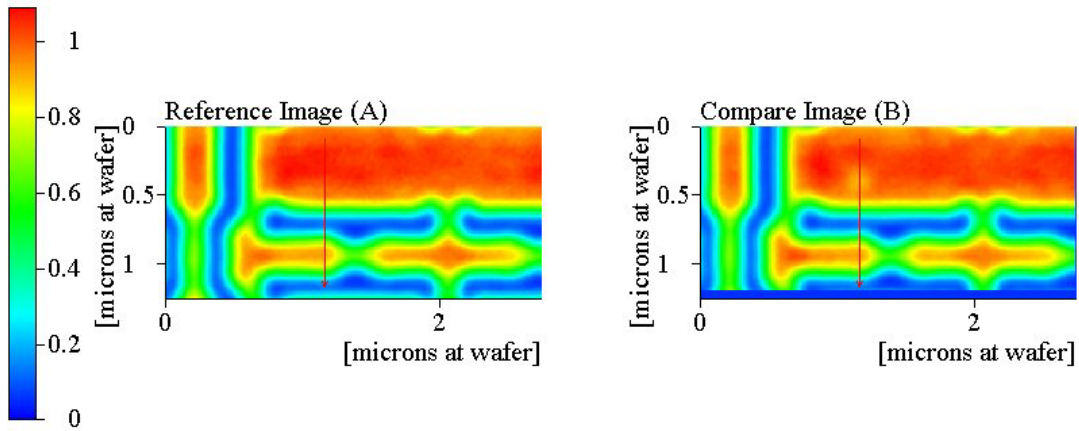


Figure 10b: Magnified AIMSTM image of the crystal growth defect of figure 10a and a reference image without defect.

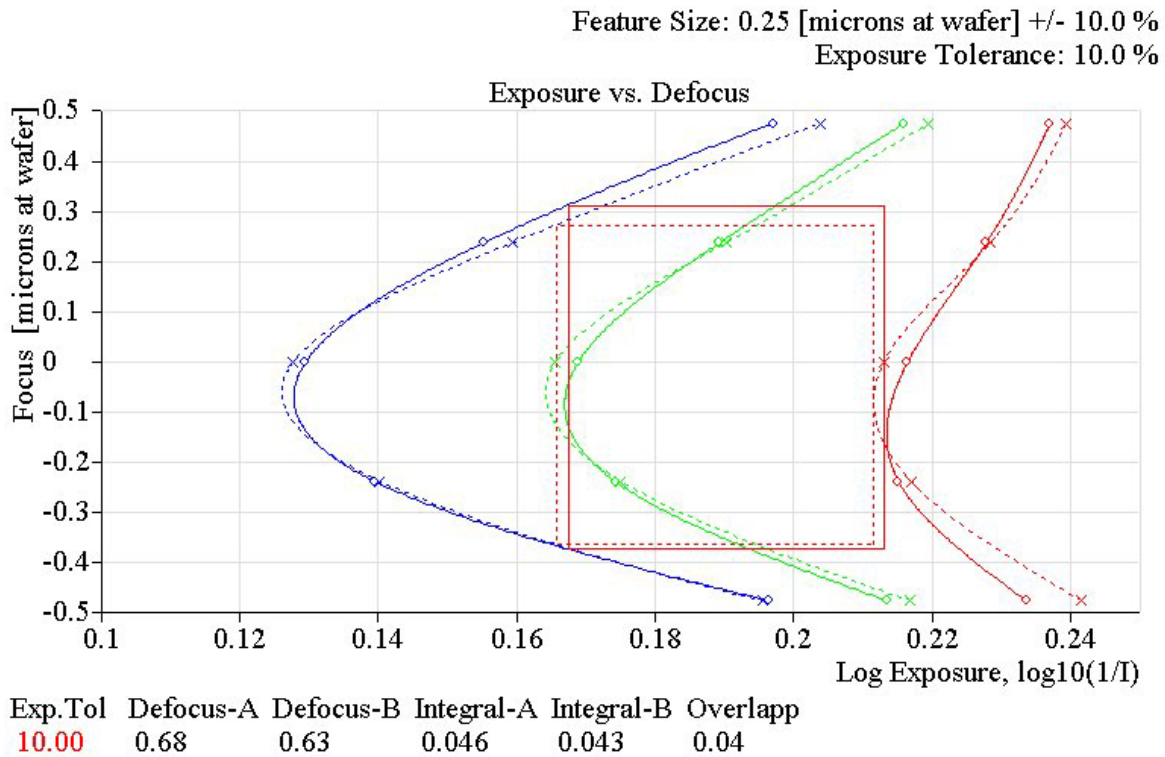


Figure 10c: Exposure-defocus-matrices of the pattern with crystal growth defect and the pattern without defect of figure 10b. The process windows overlap well showing that the defect has little impact on the lithography process.

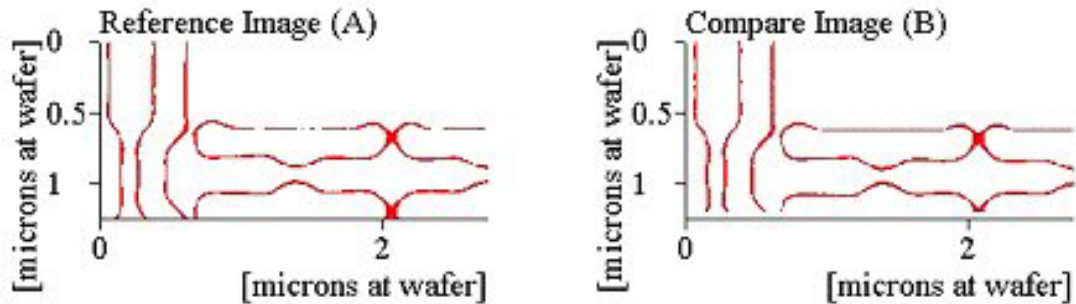


Figure 10d: Contour plots of the pattern with crystal growth defect and the pattern without defect of figure 10b based on a straightforward threshold model. This visualizes that this crystal growth is a non-printing defect.

5. CONCLUSION

The Advanced Reticle Defect Disposition (ARDD) process with the new ETHERCOMM connectivity between the surface inspection (TeraSTAR) and aerial image (AIMS™) review stations was applied successfully for the first time. In our study we focused on the detection and the assessment of the printability of crystal growth or progressing defects. It was found that crystal growth defects generate a significantly different transmission loss at different lithography settings, in various cases making them a printing defect with some settings and a non-printing defect with others. This shows that generic disposition criteria like defect size are not sufficient and that a review station emulating stepper/ scanner settings at the actinic wavelength is required to determine their printability. Furthermore, to accurately assess the impact on the process window (defocus-exposure-matrix) of crystal growth defects located close to printing patterns, through-focus evaluation of the aerial image at actinic wavelength is required in order to optimize the disposition process. Both features, exact settings of the lithographic process and through focus evaluation, are important components of an overall effective and economical reticle monitor strategy, e.g. in order to optimize the reticle cleaning cycles and thus prolong the reticle lifetime.

ACKNOWLEDGEMENTS

The authors would like to thank Christian Ziernberg for his dedicated measurement support and Ben Eynon, Andrew Ridley, Peter Schaeffer, Thomas Scheruebl and Uwe Horn for very valuable discussions related to the topic.

REFERENCES

1. V. Shea, W. J. Wojcik, *Pellicle cover for projection printing system*, US Patent 4, 131, 363, December 26, 1978
2. J. S. Gordon, *Pellicles designed for high performance lithographic processes*, SPIE, Vol. 2512, pp. 99-111, 1995
3. B. J. Grenon, C. R. Peters, and K. Bhattacharyya, *Tracking down causes of DUV sub-pellicle defects*, Solid State Technology, June 2000
4. A.M. Zibold, R. Schmid, B. Stegemann, T. Scheruebl, W. Harnisch, Y. Kobiyama, *Aerial image measurement technique for Automated Reticle Defect Disposition (ARDD) in wafer fabs*, Proceedings of SPIE Vol. 5446-117, 2004.
5. R.A. Budd, D.B. Dove, J.L. Staples, R.M. Martino, R.A. Ferguson, J.T. Weed, *Development and application of a new tool for lithographic mask evaluation, the stepper equivalent Aerial Image Measurement System, AIMS*, IBM J. Res. Develop. Vol 41 No.1, 2 January/ March, 1997.
6. R.A. Budd, J. Staples and D. B. Dove, *A New Tool for Phase Shift Mask Evaluation, the Stepper Equivalent Aerial Image Measurement System AIMS*, Proceedings of SPIE Vol. 2087, 1993.
7. K. Bhattacharyya, William Volk, Brian Grenon, Darius Brown and Javier Ayala, *Investigation of reticle defect formation at DUV lithography*, BACUS Symposium on Photomask Technology, 2002.